Climate Dynamics (2020) 55:3239–3252
https://doi.org/10.1007/s00382-020-05444-7

Identifying the sources of seasonal predictability based on climate memory analysis and variance decomposition

Da Nian[1] · Naiming Yuan[2,3] · Kairan Ying[3] · Ge Liu[4] · Zuntao Fu[1] · Yanjun Qi[4] · Christian L. E. Franzke[5]

Received: 18 September 2019 / Accepted: 23 August 2020 / Published online: 3 September 2020

Abstract

It is well recognized that climate predictability has three origins: (i) climate memory (inertia of the climate system) that accumulated from the historical conditions, (ii) responses to external forcings, and (iii) dynamical interactions of multiple processes in the climate system. However, how to systematically identify these predictable sources is still an open question. Here, we combine a recently developed Fractional Integral Statistical Model (FISM) with a Variance Decomposition Method (VDM), to systematically estimate the potential sources of predictability. With FISM, one can extract the memory component from the considered variable. For the residual parts, VDM can then be applied to extract the slow varying covariance matrix, which contains signals related to external forcings and dynamical interactions of multiple processes in climate. To demonstrate the feasibility of this new method, we analyzed the seasonal predictability in observational monthly surface air temperatures over China from 1960 to 2017. It is found that the climate memory component contributes a large portion of the seasonal predictability in the temperature records. After removing the memory component, the residual predictability stems mainly from teleconnections, i.e., in summer the residual predictability is closely related to sea surface temperature anomalies (SSTA) in the eastern tropical Pacific and the northern Indian Ocean. Our results offer the potential of more skillful seasonal predictions compared with the results obtained using FISM or VDM alone.

Keywords Seasonal potential predictability · Seasonal predictability sources · Long-term memory · Variance decomposition

1 Introduction

Successful seasonal climate predictions are crucial for a variety of fields including the early warning of disasters, agriculture, fisheries, diseases control, and resource management, etc. (Choi et al. 2015; MacLeod et al. 2015; Tadesse et al. 2016; Franzke 2017; Tommasi et al. 2017; Thornton et al. 2019). Compared with weather forecasting and climate change diagnosis, seasonal climate predictions are more difficult due to the elusive nonlinear effects among multiple processes at different scales. With the development of new theories and methods (including both dynamical and statistical models) during the past years, the skill of seasonal climate predictions has been improved, mainly in the tropics where the sources of predictability [e.g. El Niño-Southern Oscillation, ENSO) are easier to be captured (Smith et al. 2012; Kim et al. 2012)]. In the extratropical regions, however, the predictive skill declines rapidly with the increase of lead time (Chen et al. 2010; Yuan et al. 2011; Kim et al. 2012; Doi et al. 2016). In some regions, the predictive skill

Electronic supplementary material The online version of this article (https://doi.org/10.1007/s00382-020-05444-7) contains supplementary material, which is available to authorized users.

✉ Naiming Yuan
naimingyuan@hotmail.com

Kairan Ying
yingkr@tea.ac.cn

[1] Lab for Climate and Ocean-Atmosphere Studies, Department of Atmospheric and Oceanic Sciences, School of Physics, Peking University, Beijing 100871, China

[2] School of Atmospheric Sciences, Sun Yat-sen University, Zhuhai 519082, China

[3] CAS Key Laboratory of Regional Climate Environment for Temperate East Asia, Institute of Atmospheric Physics, Chinese Academy of Sciences, Beijing 100029, China

[4] Chinese Academy of Meteorological Sciences, Beijing 100081, China

[5] Meteorological Institute, and Center for Earth System Research and Sustainability, University of Hamburg, Hamburg, Germany

even vanishes when the lead time is longer than 1 month (Smith et al. 2012; Baehr et al. 2015; Pokhrel et al. 2016). One reason for the current difficulty is that the relations between the prediction objects and the precursory factors are not always stable. For a prediction object, many precursory factors may be proposed (Liu and Fan 2012; Duan et al. 2013; Liu and Duan 2017), but it is difficult to determine which factor works constantly well. Moreover, the prediction models usually show reduced predictive skills comparing to the hindcast skills. These situations may be attributed to the lack of sufficient knowledge on the sources of predictability. Accordingly, identifying and understanding the sources of seasonal predictive skill in the extratropics has become an important issue.

It has been well recognized (National Research Council 2010; National Academies of Sciences, Engineering, and Medicine 2016) that there are three sources of climate predictability: (i) the inertia or memory of climate variables that are accumulated from past conditions, (ii) the responses to external forcings including volcanic eruptions, etc., and (iii) the multiple interactions among different processes in terms of feedbacks, teleconnections, etc. During the past years, a number of studies have been carried out to explore the potential relationships between the targeted climate patterns/variables and (i) external forcings, as well as (ii) the dynamical mechanisms of different interactions of coupled systems (Brunet et al. 2010; Davies 2015; Ying et al. 2017; He et al. 2018). However, little attention has been paid to the effects of climate memory until recently when the fractional integral techniques were introduced to the studies of climate memory (Yuan et al. 2014, 2019; Lovejoy et al. 2015). As a result, the potential predictability reported by previous studies may be from mixed predictable sources (e.g., a mixture of the effects from climate memory and teleconnections), which could further increase the uncertainties of the subsequent climate predictions.

To clarify the different sources of the seasonal predictability, one potential solution is to identify the contributions of different sources one by one. For example, we may first estimate the climate memory effects. After removing the memory component from the considered variable, the potential predictability from the other sources can then be explored in the residual part. For the memory part, it has been widely recognized that many variables such as temperature, relative humidity, and winds, among others, are characterized by climate memory (Koscielny-Bunde et al. 1998; Kurnaz 2004; Chen et al. 2007; Vyushin and Kushner 2009). This memory is normally termed as "Long-term memory (LTM)" as the influences from the historical conditions may last for a long time (months, years, or even decades). It sounds counter-intuitive, but several potential mechanisms have been proposed in the past few years (Fraedrich et al. 2004; Franzke et al. 2015, 2020; Fredriksen and Rypdal 2017). The emergence of LTM is normally attributed to the ocean heat content (Fraedrich and Blender 2003; Yuan et al. 2013; Fredriksen and Rypdal 2016), and the nonlinear interactions among climate subsystems of multiple scales are believed crucial for the arising of LTM (Fredriksen and Rypdal 2017; Franzke et al. 2020). To estimate the climate predictability originated from climate memory, a new model, Fractional Integral Statistical Model (FISM), was proposed (Yuan et al. 2013, 2014), with which the influences accumulated from the past can be extracted quantitatively as,

$$x_t = M_t + R_t, \tag{1}$$

where M_t stands for the extracted memory part and R_t denotes the residual forcing part. It has been reported that the stronger climate memory is, the higher the explained variance by M_t is, indicating stronger predictability (Yuan et al. 2019).

Regarding the other two sources of climate predictability (i.e. responses to external forcings, effects of teleconnections, etc.), one can then focus on the residual forcing part R_t to detect the additional potential predictability. For this purpose, a variance decomposition method (VDM) developed by Zheng and Frederiksen (2004) may be appropriate. Based on monthly data, the VDM is designed to extract the fast (unpredictable) component of interannual variability arising from the intraseasonal variability and the slow (potential predictable) component of interannual variability arising from slow varying processes on interannual or longer timescales. The potential seasonal predictability is thus defined as the proportion of the variability that is explained by the slow varying component. This method has been widely used in estimating the seasonal predictability of different variables (Ying et al. 2013, 2015, 2016, 2017; Frederiksen et al. 2018). After identifying the slow varying (predictable) component, the VDM also allows the identification of the sources of the predictability in R_t using traditional statistical methods such as the Empirical Orthogonal Function (EOF) analysis, the linear regression analysis, etc. However, it is worth noting that the VDM by itself does not distinguish between the predictability by climate memory and the predictability from other sources.

Following the above strategy, we combine the FISM and the VDM together and develop a new method, the Fractional Integral-Variance Decomposition Method (FI-VDM). The new method inherits the advantages of both the FISM and the VDM, and is able to identify the sources of seasonal predictability with climate memory effects properly considered. In fact, it should be noted that the climate predictability sourced from climate memory is not independent of the other two sources. For instance, recent studies have reported that external forcings (i.e. volcanic forcings) may strengthen the observed LTM in

the climate system (Vyushin et al. 2004; Fredriksen and Rypdal 2017; Qiu et al. 2020), and the interactions among different processes of multiple scales (i.e. sea–air interactions) may contribute to the arising of LTM. Accordingly, the predictability estimated from climate memory may overlap with the predictability of other origins, and the additional potential predictability revealed from the residual forcing part R_t corresponds to specific processes that are not covered by climate memory. Using this new method, we estimate the seasonal predictability of the observed monthly surface air temperatures over China. It is found that the climate memory contributes already a large portion of the seasonal predictability. After removing the effects of climate memory, other sources of predictability including sea surface temperature anomalies (SSTA) in the eastern tropical Pacific and the northern Indian Ocean are also revealed. With all these predictable sources identified, an improved seasonal prediction may be expected.

The remainder of this paper is organized as follows. In Sect. 2, the data used in this study will be introduced, and the methods including FISM, VDM, and the combined new method FI-VDM will then be described. In Sect. 3, the seasonal predictability of the observed monthly surface air temperatures over China will be estimated to show the usability of the new method FI-VDM, and the sources of seasonal predictability will be identified. After comparing the results obtained from FI-VDM and those obtained from VDM, in Sect. 4, we provide a discussion and conclusions.

2 Data and methods

2.1 Data

In this study, the observed monthly mean surface (2 m) air temperature records from 1729 meteorological stations over China (colored circles in Fig. 1) are analyzed to demonstrate the usability of the FI-VDM. These records are obtained from the China Meteorological Administration and cover the period January 1960 to December 2017. The records are standardized by removing the seasonal cycle (Koscielny-Bunde et al. 1998), as $x_t = \tau_t - < \tau_t >, t = 1, \ldots, N$, where $\{\tau\}$ is the observed data, N is the data length, and $< \tau_t >$ is the long-time average for each calendar month. Besides the observed temperature records, we also use the monthly mean sea surface temperatures (SSTs) on a $1.0^o \times 1.0^o$ grid of HADISST1.1 dataset from Met Office Hadley Centre for the same time period (Rayner et al. 2003). The data is downloaded from https://www.metoffice.gov.uk/hadobs/hadisst/data/download.html.

2.2 Methods

2.2.1 Fractional integral statistical model (FISM)

To estimate the climate memory effects, we employ the fractional integral statistical model (FISM) to extract the memory part M_t as introduced in Eq. (1). The FISM is a generalized version of the stochastic climate model (SCM) proposed by (Hasselmann 1976). From the SCM, it is suggested that the slow varying processes of the climate system can be considered as

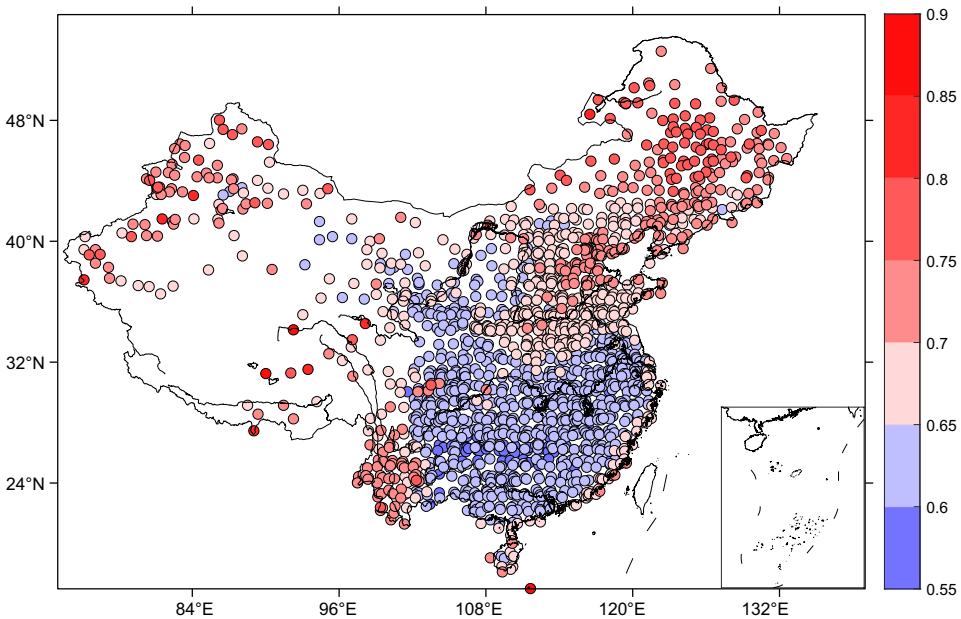

Fig. 1 The spatial distribution of the 1729 meteorological stations where the surface (2 m) air temperatures are analyzed in this study. The color of each circle represents the α value obtained from DFA3

the accumulative responses to continual random excitations by short term disturbances on weather scales. Following this concept, Yuan et al. (2013, 2014) found that the long-lasting influences from the past [the memory part, M_t in Eq. (1)] and short term disturbances [the residual forcing part, R_t in Eq. (1)] can be connected via Riemann-Liouville Fractional integral formula, as shown below (Yuan et al. 2014),

$$M_t = \frac{1}{\Gamma(q)} \int_{u=0}^{t-\delta} \frac{R_u}{(t-u)^{1-q}} \mathrm{d}u, \tag{2}$$

and the Eq. (1) can be written as,

$$x_t = \frac{1}{\Gamma(q)} \int_{u=0}^{t-\delta} \frac{R_u}{(t-u)^{1-q}} \mathrm{d}u + R_t, \tag{3}$$

where R_u ($u = 0, \delta, 2\delta, \ldots, t-\delta$) denotes the historical forcing part and R_t the forcing part at the present time t (δ is the sampling time interval). Γ is the gamma function. $t-u$ represents the distance between historical time point u and the present time t. The parameter q denotes the order of the fractional integration, which can be estimated from the Detrended Fluctuation Analysis (DFA). DFA is a widely used method to measure the strength of climate memory (Peng et al. 1994; Koscielny-Bunde et al. 1998; Kantelhardt et al. 2001; Chen et al. 2007; Rybski et al. 2008; Yuan et al. 2015; Jiang et al. 2017). By applying DFA to the observed time series x_t, one can calculate the fluctuation function $F(s)$ on different time scales s, and estimate the DFA exponent α as the slope of $F(s)$ versus s in a log-log plot. As shown in Fig. 2a, if there is indeed a scaling behavior between $F(s)$ and s as $F(s) \sim s^{\alpha}$, and the exponent α is larger than 0.5, one can say that there is long-term climate memory in the considered variable (see also Fig. 1 for the spatial distribution of the α values). For more details about the DFA method, please refer to Peng et al. (1994), Kantelhardt et al. (2001). It has been found that the DFA exponent α is linearly related with q as $q = \alpha - 0.5$ (Yuan et al. 2014). From Eq. (3), one can see that x_t is influenced by both the present forcing part R_t and the historical forcing part R_u. The decay of the influences from R_u (with time) can be simulated using the fractional integration, which depends on only one parameter q (Yuan et al. 2013). Specifically, Eq. (3) can be written into its discrete form,

$$x_t = \sum_{u=0}^{t-\delta} k(q;t-u) R_u + R_t, \tag{4}$$

where $k(q;t-u) = \frac{1}{\Gamma(q)(t-u)^{1-q}}$, represents the memory kernel of the considered variable. After estimating q from the observed variable x_t (using DFA), the memory kernel can be estimated. Assuming $R_0 = x_0$, the historical forcing part R_u ($u = 0, \delta, 2\delta, \ldots, t-\delta$) can be extracted from x_t by reversely solving Eq. (4), as shown below,

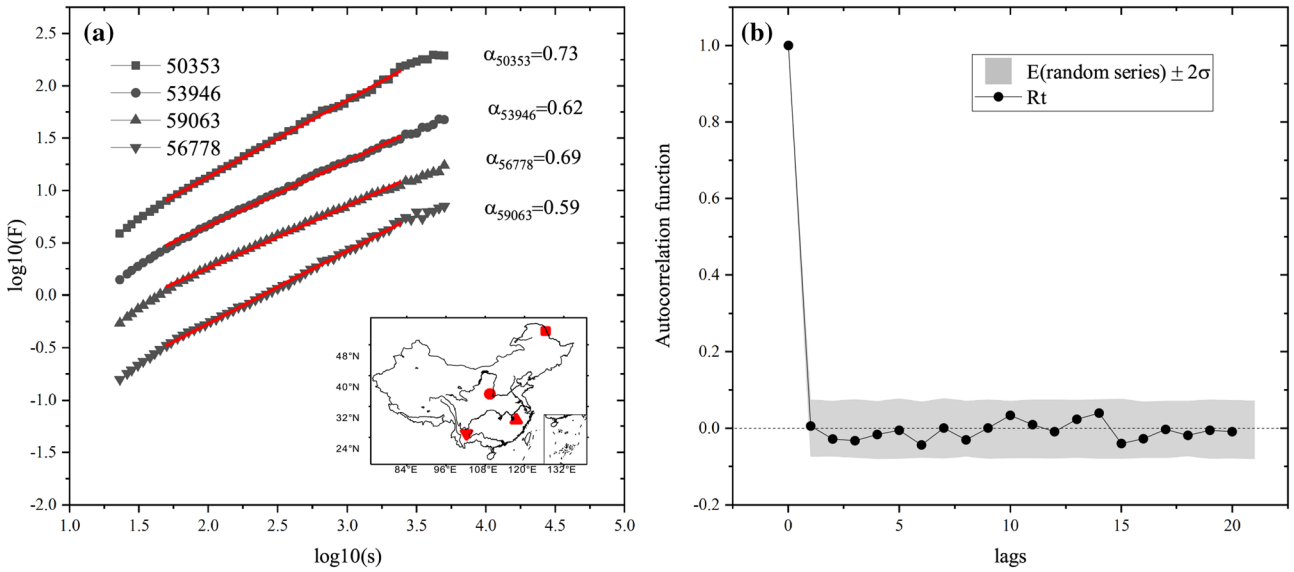

Fig. 2 **a** The DFA results of the temperature records observed from four representative stations of different locations. The DFA exponent α measures the strength of the climate memory. $\alpha > 0.5$ indicates the existence of long-term climate memory. The four stations are Huma (station No. 50353), Huanglong (station No. 53946), Jianghua (station No. 59063) and Kunming (station No. 56778). **b** The autocorrelation functions of the residual forcing part R_t. The autocorrelations are averaged over all the 1729 stations (see Fig. 1). The gray area indicates the uncertainties (two times of standard deviation) of the autocorrelations when random series are considered

$$
\begin{aligned}
&R_0 = x_0\\
&R_\delta = x_\delta - k(q;\delta)R_0\\
&R_{2\delta} = x_{2\delta} - k(q;2\delta)R_0 - k(q;\delta)R_\delta\\
&\cdots\\
&R_{t-\delta} = x_{t-\delta} - \sum_{u=0}^{t-2\delta} k(q;t-\delta-u)R_u.
\end{aligned}
\tag{5}
$$

It is worth noting that the assumption $R_0 = x_0$ ignored the potential influences before the starting point of the considered time series. As a result, the extracted historical forcing part may be biased at a few points in the beginning. To avoid this deviation, we remove the first 2 years (24 months) data and mainly focus on the residual forcing part from 1962 to 2017. It has been tested that the relative errors of the estimated R_u from 1962 are already smaller than 5% (figures not shown).

With R_u derived, the memory part M_t can thus be calculated using Eq. (2). The climate memory effects, or in other words, the potential predictability contributed by the climate memory, can thus be estimated as

$$P_M = \frac{V(M_t)}{V(x_t)}, \tag{6}$$

assuming M_t and R_t are independent (Xie et al. 2019). In this equation, "V" means the variance of the corresponding component. Note that although the estimated predictability in terms of climate memory may overlap with the predictability of other origins (see the introduction above), there may still be some processes that do not contribute to the arising of LTM, but are meaningful for climate prediction. To further explore the extra potential predictability from other sources, one needs to focus on the residual forcing part R_t.

2.2.2 Variance decomposition method (VDM)

To explore the potential predictability from R_t, we employed the variance decomposition method (VDM) that was proposed by Zheng and Frederiksen (2004). Suppose we have a R_{ym} in month m ($m = 1, 2, 3$; m is a specific month) and in year y ($y = 1, 2, 3, \cdots, Y$, where Y is the total number of years), in VDM, the R_{ym} is conceptually decomposed into two components including a seasonal "population" mean μ_y and a residual departure from this mean ε_{ym},

$$R_{ym} = \mu_y + \varepsilon_{ym}, \tag{7}$$

where the month-to-month fluctuations, or intraseasonal variability, arises entirely from ε_{ym}. By calculating the seasonal mean of R_{ym} and ε_{ym} over the three months of a given season (e.g., spring), Eq. (7) can be written as,

$$R_{yo} = \mu_y + \varepsilon_{yo}, \tag{8}$$

where the subscript "o" indicates the seasonal mean. In this equation, ε_{yo} is the fast or unpredictable component as it is related to intraseasonal events, and μ_y represents the slow or predictable component that is associated with external forcing and slow varying internal dynamics on interannual or longer timescales. After estimating the interannual variances of ε_{yo}, R_{yo}, and μ_y [see Eqs. (16–19) in Zheng and Frederiksen (2004)], the potential predictability in seasonal mean R_t can be calculated as,

$$P_R = \frac{V(\mu_y)}{V(R_{yo})}, \tag{9}$$

assuming μ_y and ε_{yo} are independent (Zheng and Frederiksen 2004). Besides calculating the variances of the three terms in Eq. (8), one could also calculate the covariances, i.e., $V(\varepsilon_{yo}, \varepsilon'_{yo})$, $V(R_{yo}, R'_{yo})$, and $V(\mu_y, \mu'_y)$, where the apostrophe indicates the variable at a different location. In this way, the covariance matrix of the predictable slow component can be obtained, which is useful for further analysis (e.g., EOF analysis) to identify the predictable modes and their sources of predictability.

It is worth noting that there is an assumption in VDM, that the intraseasonal components are uncorrelated if they are a month or more apart. This assumption is well satisfied by R_t (Fig. 2b). In addition to exploring potential predictability from the residual forcing part R_t, the VDM can also be applied directly to the original time series x_t, in which case the climate memory part is not removed beforehand. For more details of the variance decomposition method, we refer to Zheng and Frederiksen (2004).

2.2.3 Fractional integral-variance decomposition method (FI-VDM)

To better estimate the seasonal potential predictability and identify the sources of predictability, the above two methods FISM and VDM are combined as FI-VDM. The strategy is to first estimate the climate memory effects using FISM, and then explore other sources of predictability using VDM. Suppose we have a measurement of a climate variable x_{ym} in month m and in year y. The work flow to apply FI-VDM is illustrated in Fig. 3, and the procedure is summarized below,

1. Decompose the x_{ym} into the memory part M_{ym} and the residual forcing part R_{ym} using FISM (Eq. (1)).
2. Apply VDM to the residual forcing part R_{ym}. For a given season (e.g., spring), estimate the total variance $V(R_{yo})$ and the variance of the predictable slow component $V(\mu_y)$.
3. Determine the total potential predictability as,

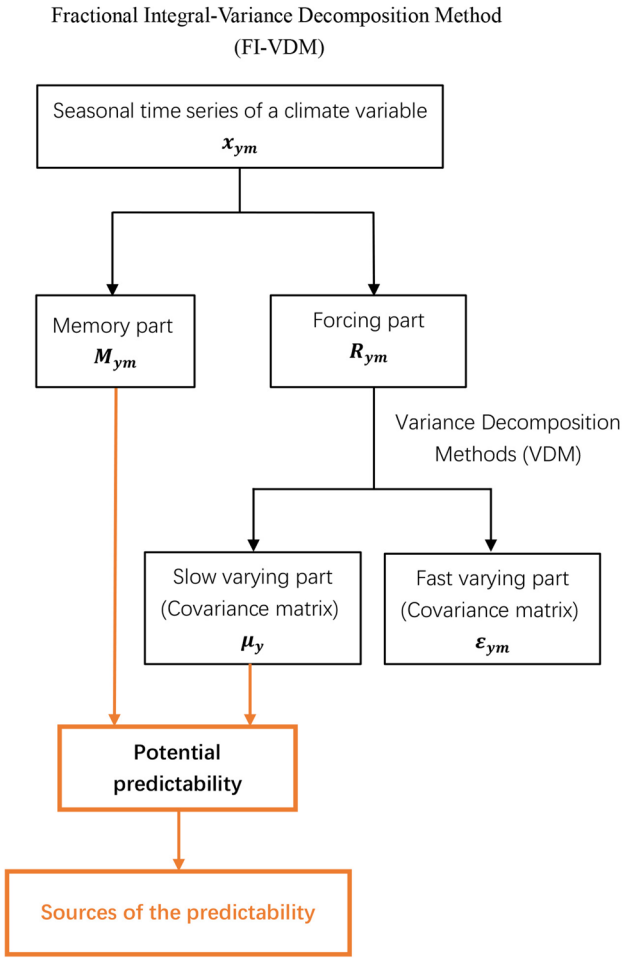

Fig. 3 Work flow of the Fractional Integral-Variance Decomposition Method (FI-VDM)

$$P = \frac{V(M_{yo})}{V(x_{yo})} + \frac{V(\mu_y)}{V(R_{yo})} * \frac{V(R_{yo})}{V(x_{yo})}, \tag{10}$$

where the first term on the right hand side stands for the seasonal potential predictability estimated from the climate memory, and the second term represents the additional contributions from other sources.

4. Calculate the covariance matrix of the predictable slow component (e.g., $V(\mu_y, \mu_y')$) using data from different locations. Apply an EOF analysis to the slow covariance matrix to detect the leading modes of the slow component. The corresponding principal component (PC) time series is calculated by projecting R_{yo} onto the slow EOF mode. Finally, identify the sources of predictability via traditional linear regression analysis.

3 Results

3.1 Potential seasonal predictability of temperature over China

To demonstrate the feasibility of the new method FI-VDM, the potential predictability of monthly mean surface air temperature records over China is studied. Before using the FISM to extract the memory part in the temperature records, we first apply DFA of the third order [DFA3, see Kantelhardt et al. (2001)] to measure the strength of the climate memory. The results are not sensitive to the selection of the DFA order. DFA2 gives qualitatively the same results. We calculated the α values for all the 1729 stations (see the colored circles in Fig. 1). Their spatial distribution is similar to previous studies (Jiang et al. 2012). Figure 2a shows the DFA results of four representative stations. It is found that the memory strength varies over different stations, but the DFA exponents are all larger than 0.5, indicating the existence of long-term climate memory. Using the α values, the fractional integration order q in the FISM is calculated, and the climate memory part is extracted. The potential predictabilities of different seasons contributed by the climate memory are shown in Fig. 4a–d (the left column). It is found that the distributions of the predictability are similar to the distribution of the α values (Fig. 1). This is reasonable as the predictability from climate memory is theoretically determined by the memory strength (Yuan et al. 2019). During all seasons, the predictabilities are stronger over southwest China, while weaker over southeast China. In the north of China, stronger predictability is found in spring (March, April, and May, MAM), summer (June, July, and August, JJA), and autumn (September, October, and November, SON), but not in winter (December, January, and February, DJF). In general, the potential predictability calculated from climate memory are stronger in spring and summer. In winter, however, the potential predictability is weak over most regions of the country. On average, the explained variance by climate memory is less than 15% in winter.

After removing the memory part, the residual forcing part R_{ym} is further analyzed. Using DFA, the residual forcing part is found to have no LTM. On average, the DFA exponent $\alpha = 0.5 \pm 0.04$, indicating a successful removal of the LTM (Fig. S1). By applying the VDM, the potential predictability in the residual forcing part is calculated. As shown in Fig. 4e–h (the middle column), the slow varying component in R_{ym} only explains a limited amount of variance, indicating weak predictability. From a Monte-Carlo tests (i.e., applying the VDM to 1729 white noises of the same length as R_{ym}), a threshold of 0.20 is suggested as the upper bound of the uncertainty interval (two times

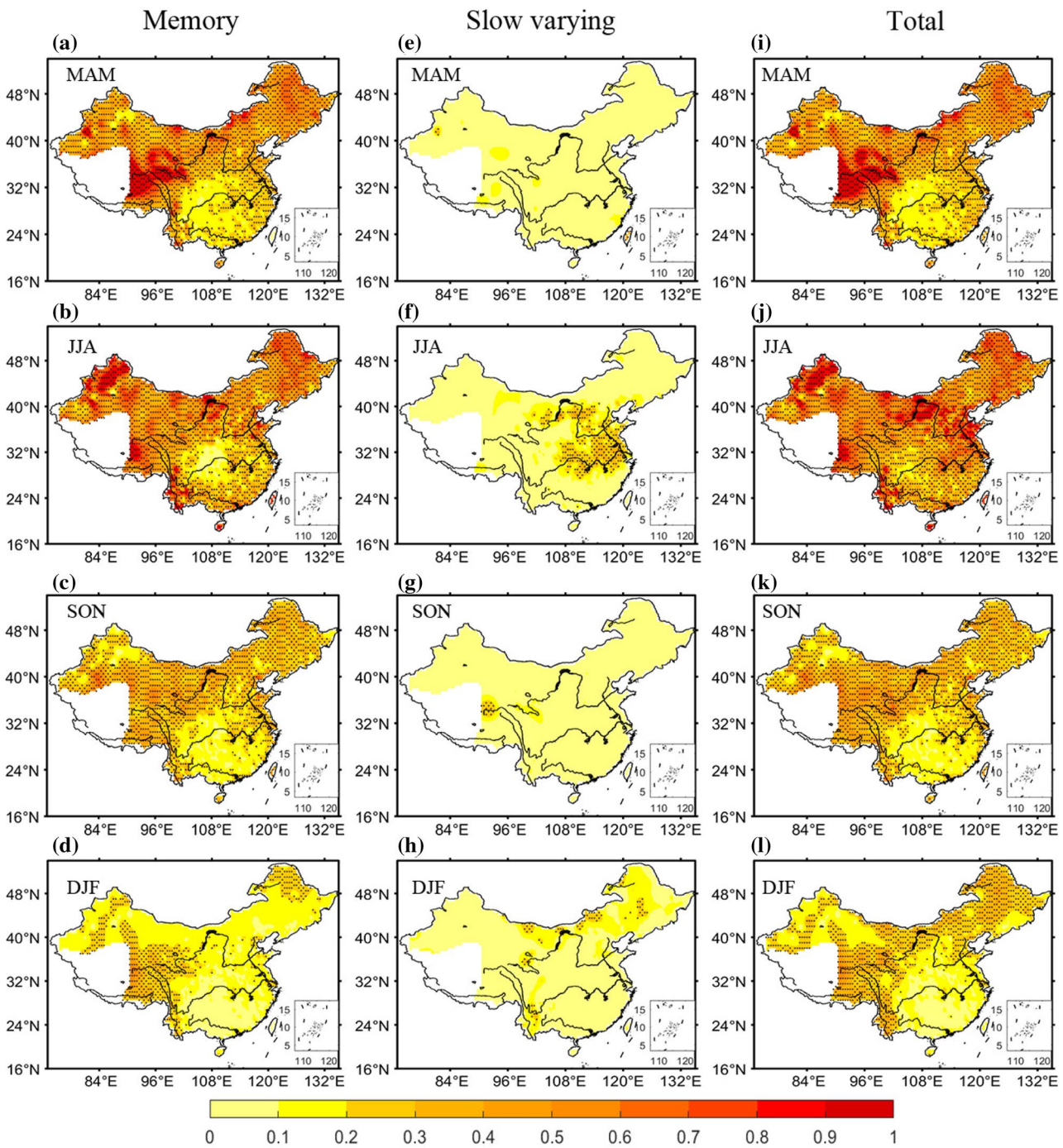

Fig. 4 Spatial distributions of the seasonal potential predictability estimated from the climate memory (**a**–**d**), the slow varying component in the residual forcing part R_{ym} (**e**–**h**), as well as the total predictability (**i**–**l**). From the top to the bottom are the results of the four seasons: spring (March–April–May, MAM), summer (June–July–August, JJA), autumn (September–October–November, SON), and winter (December–January–February, DJF). The shading areas indicate the regions with the estimated predictability larger than 0.20. The climate memory effects contribute to a large portion of the total predictability. As a result, the predictability from the residual forcing part R_{ym} is much weaker, but there are still additional predictability revealed, e.g., in summer (**f**)

standard deviation from the mean value) in the results of white noises. Accordingly, the potential predictability is not statistically significant in most areas. This is reasonable as a large portion of the slow varying component in the original temperature anomalies x_{ym} has been removed in terms of M_t. As introduced above, the climate memory effect is not independent from the other sources of the predictability. M_t represents the effects accumulated from

past times, which also contribute to the slow varying component. In spite of this, however, there are still regions highlighted with meaningful predictability patterns in R_{ym}. Particularly in the region around the middle/lower reaches of the Yangtze River and the Huai-River basin in summer (see the shading area in Fig. 4f), after the removal of the climate memory part M_t, no significant LTM is detected in the residual forcing part R_t (Fig. S1), but there are still additional sources of predictability, which might be related to external forcings or multiple interactions among different processes in terms of teleconnections, feedbacks, etc.

Using Eq. (10) the potential predictability from both the climate memory and the slow varying component in R_{ym} are combined together as the potential total predictability (Fig. 4i–l, the right column). In general, the surface air temperatures in the north and the southwest of China exhibit stronger seasonal predictability, with P larger than 0.40 in a large part of the area. In southeast China, the temperature is relatively less predictable in spring, autumn, and winter. For these three seasons, the seasonal predictability P is normally smaller than 0.20 in south of the Yangtze River. The strongest seasonal predictability is found in summer (Fig. 4j), and the P values are larger than 0.5 in many regions over the country. By comparing the potential total predictability with the results from FISM, it is found that climate memory makes a large contribution to total predictability. As shown in Table 1, the predictability from climate memory on average accounts for more than 90% of the potential total predictability in spring ($0.37/0.38 = 97.4\%$) and autumn ($0.28/0.29 = 96.6\%$). In summer and winter, the percentages accounted by climate memory is smaller, but are still larger than 70%. This finding is in line with the introduction above, that the climate predictability sourced from climate memory overlaps with the predictability of other origins. Since we considered the climate memory effects first, it is reasonable that a larger proportion of the climate predictability is identified in terms of climate memory. It is worth noting that the climate memory effects do not dominate the total predictability in all regions. In the middle/lower reaches of the Yangtze River, for instance, the memory strength is low (Fig. 1), but the seasonal predictability is strong (Fig. 4j). Accordingly, besides climate memory effects, other sources of predictability also deserves attention. In winter, although there is around 28.6% of the potential total predictability originated from the residual forcing part (Table 1), the absolute value of the average predictability in winter is only 0.06, and there are very few areas with local extra predictability exceeding 0.20 (Fig. 4h). Therefore, we will only focus on the residual forcing part R_{ym} in summer temperatures, where the average predictability is relatively high, and some key regions (i.e., the middle/lower reaches of the Yangtze River and the Huai-River basin) have been highlighted with significant potential predictability (Fig. 4f). The identification of the sources is discussed next.

Table 1 The average seasonal potential predictability of the surface air temperatures over China

Season	$P(M_{ym})$	$P(R_{ym})$	Predictability
MAM	0.37	0.01	0.38
JJA	0.42	0.12	0.54
SON	0.28	0.01	0.29
DJF	0.15	0.06	0.21

$P(M_{ym})$ represents the predictability explained by the climate memory effects. $P(R_{ym})$ denotes the predictability extracted from the residual forcing part R_{ym}. The four seasons are: spring (March–April–May, MAM), summer (June–July–August, JJA), autumn (September–October–November, SON), and winter (December–January–February, DJF)

3.2 Sources of seasonal predictability of summer temperatures over China

To the end of this section, the slow varying components revealed in the residual forcing part R_{ym} will be studied in detail. As introduced in the Sect. 2.2, in VDM one could not only calculate the variance of the slow varying component $V(\mu_y)$, but also the covariance $V(\mu_y, \mu_y')$ using data from different locations. This means a covariance matrix of the predictable slow varying component can be obtained, which allows a further EOF analysis for the leading mode and the PC time series of the slow component. In this way, the potential sources of predictability may be identified using traditional diagnostic methods (e.g. linear regression). Following this research route, we identify the predictable sources in R_{ym} for summer (JJA) temperatures over China.

Figure 5a shows the leading predictable mode of the slow varying component in R_{ym} for summer. Similar to Fig. 4f, the middle/lower reaches of the Yangtze River and the Huai-River basin are highlighted in this mode, indicating stronger potential predictability. By calculating the correlations between the corresponding PC time series and the sea surface temperature anomalies (SSTA) at different time lags (Fig. 5b–e), significant negative correlations are found in the northern Indian Ocean and the eastern equatorial Pacific, indicating the possible influence from the Indian Ocean Basin (IOB) pattern and the ENSO. These SSTA signals arise 3 months (Fig. 5b, see also Fig. S2) before the leading mode in Fig. 5a, and become stronger over time (Fig. 5c–e). They may correspond to the well known Indo-western Pacific ocean capacitor (IPOC) effect, which may contribute to the predictability of the summer-time East Asian climate (Li et al. 2013; He and Wu 2014; Xie et al. 2016). As proposed in previous studies (Liu et al. 2016; Xie et al. 2016), ENSO induces coherent climate anomalies over the Indo-western Pacific, which further excite a tropospheric

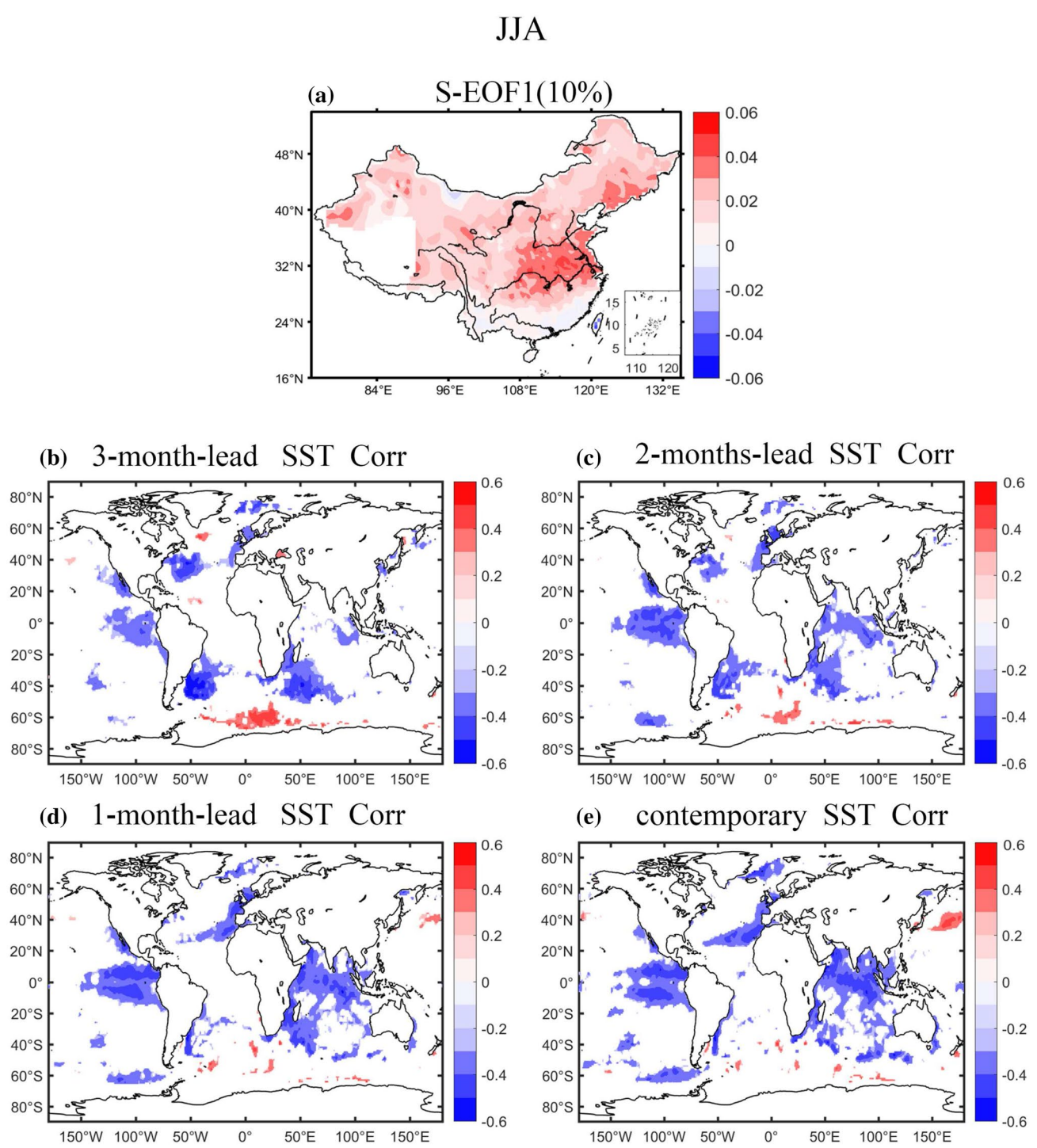

Fig. 5 Potential sources of the predictability for the residual forcing part R_{ym} in summer. **a** The spatial patterns of the leading EOF calculated from the covariance matrix of the slow varying component in R_{ym}. The corresponding PC time series is used to calculate the correlations with the sea surface temperature (SST) anomalies of different time lags: **b** the SST anomalies (March–April–May, MAM) lead by 3 months, (c) the SST anomalies (April–May–June, AMJ) lead by 2 months, **d** the SST anomalies (May–June–July, MJJ) lead by 1 month, and **e** the SST anomalies (June–July–August, JJA) are contemporary with the PC time series. The colored areas indicate regions with significant correlations at the 95% confidence level. The sources of the predictability are mainly found over the eastern tropical Pacific and the northern Indian Ocean

kelvin wave propagating into the western Pacific, and affect East Asia in the following summer by forcing anomalous anticyclone (AAC) and Pacific-Japan (PJ) pattern. In this mechanism, the ENSO shows its role through the monsoonal Indo-Northwest Pacific, and the coherent SSTA in IOB connects the ENSO and the East Asian Climate. Accordingly, the SSTA in these two regions may serve as the source of the predictability for the summer temperatures over China. However, different from previous studies, our analysis is conducted on the residual forcing part R_{ym}, which contains no climate memory effects. Recall the potential mechanisms that multi-scale interactions are crucial for the arising of LTM, ENSO, as a member of the multi-scale interactions in the climate system, certainly would contribute to the emergence of climate memory. Therefore, the findings here indicate that even if the climate memory effects are removed, there is still additional predictability left in R_{ym}, which may arise from specific processes such as the IPOC.

To better understand the findings shown in Fig. 5, we also detect the sources of seasonal predictability in summer temperatures over China using the VDM alone. This means that the VDM is applied to the original time series x_{ym} without removing the climate memory part. As shown in Fig. 6, the leading mode of the slow varying component in x_{ym} shows a featured area in northern China (Fig. 6a), which is different from that obtained in R_{ym} (Fig. 5a). A closer look at Fig. 6a further tells us that the leading mode is similar to the distributions of the climate memory effects revealed by FISM (Fig. 4b). This means the predictable pattern detected by VDM mainly represents the potential predictability by LTM. Recall the argument that the emergence of LTM is mainly attributed to the ocean heat content, the large ocean areas highlighted in Fig. 6b–e further supported the idea that the VDM mainly reveals the climate memory effects. In other words, if only the VDM is applied, the sources of predictability revealed in the leading mode may be masked by the climate memory effects, and meaningful signals such as the IPOC effect are not easy to detect. For more meaningful patterns, one needs to go further to the other EOF modes, e.g., EOF2 (see Fig. S3). However, in this case the EOF patterns may show mixed features. For instance, the EOF2 of the slow varying component in x_{ym} (based on VDM alone) is found not identical with the leading mode of the slow varying component in R_{ym} (based on FI-VDM), but shows combined features that are partly similar to both the first and the second mode from FI-VDM. Since FI-VDM by design is able to properly consider the climate memory effects, the identified sources of predictability may be better interpreted with more reliable physical meanings. In contrast, without a proper removal of the climate memory effects, such as using the VDM alone, the different sources of predictability are not easy to be identified and the interpretations of the results may comparatively have more uncertainties.

4 Discussion and conclusion

In this study, we developed a new method, Fractional Integral-Variance Decomposition Method (FI-VDM). This method is a combination of the fractional integral statistical model (FISM) and the variance decomposition method (VDM). It is designed to estimate the seasonal potential predictability of a given climate variable, and more importantly, to identify the sources of predictability. Compared to VDM, FI-VDM inherits the advantages of FISM and is able to properly consider the climate memory effects on predictability. While better than FISM, FI-VDM could further reveal additional predictability originated from other mechanisms (e.g., feedbacks, teleconnections), which is an important complement for the estimation of potential predictability. Using this new method, the seasonal predictability in the surface air temperatures over China is studied, and the sources of the predictability are identified. It is found that climate memory in the temperature contributes already a large portion (> 70%) of the seasonal predictability. After removing climate memory effects, other sources of predictability including sea surface temperature anomalies in the eastern tropical Pacific and the northern Indian Ocean are revealed (Fig. 5). These identified sources of predictability allow us to develop a new seasonal prediction model. For instance, one may first quantify the climate memory part M_t using Eq. (2). For the residual forcing part R_t, a simple regression model may be further designed using the detected sources of predictability. In this way, with the climate memory effects properly considered, an improved seasonal prediction may be expected.

In addition to analyzing the surface air temperatures using FI-VDM, results based on the FISM and the VDM alone are also obtained for comparison (Fig. 7). Roughly speaking, the results from the three methods are similar. Both the FISM and the VDM reveal the strong seasonal predictability in the north and the southwest of China, and the weak seasonal predictability in the southeast of China. The predictability based on the FISM (Fig. 7a–d, see also Fig. 4a–d) is slightly weaker than the results from the FI-VDM (Fig. 7i–l, see also Fig. 4i–l). This is reasonable, as the estimation from the FISM only accounts for climate memory effects, while FI-VDM also includes the additional potential predictability that is left in the residual forcing part R_t. As for the VDM, the results are found more similar to those obtained from the FI-VDM. There are only tiny differences between the results, which might be due to the different assumptions of the two methods [e.g., in the VDM, the intraseasonal components in x_t are assumed to be uncorrelated if they are a month or more apart (Zheng and Frederiksen 2004); while in the FI-VDM, the memory part M_t and the residual forcing part R_t are assumed to be independent (Xie et al. 2019)]. Accordingly,

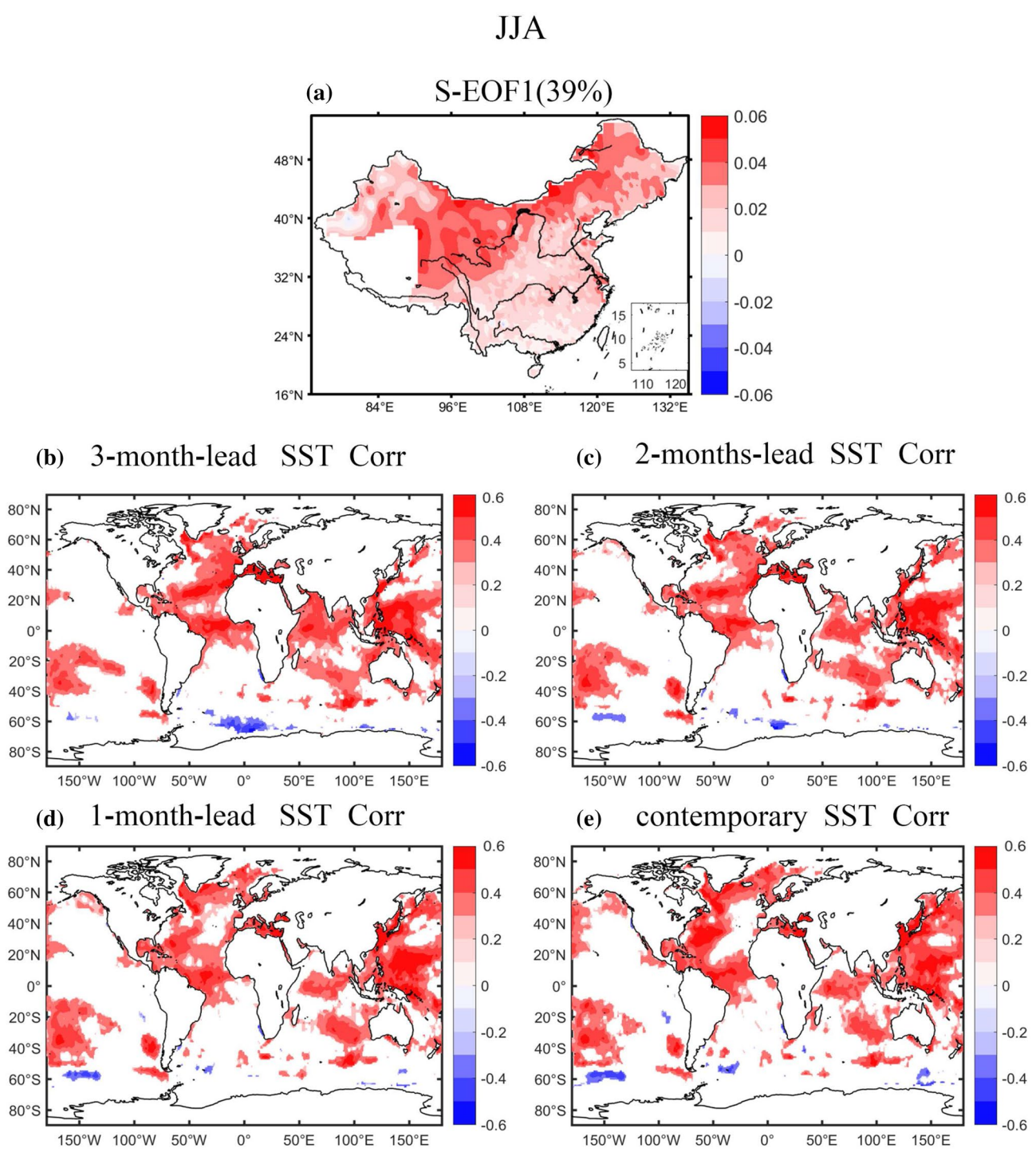

Fig. 6 Similar to Fig. 5, but the VDM is applied directly to the temperature anomalies x_t. **a** shows the spatial patterns of the leading EOF calculated from the covariance matrix of the slow varying component in x_t. **b**–**e** represent the correlations between the PC time series and the sea surface temperature (SST) anomalies with different time lags. The colored areas indicate regions with significant correlations at the 95% confidence level

from the similar patterns shown in Fig. 7, one can confirm the reliability of the VDM, and also the feasibility of the new method FI-VDM in estimating seasonal predictability. It should be noted that finding a reliable explanation for the differences between the results of the two methods is not easy. For this purpose, one has to figure out the different effects of the different assumptions, but this is beyond the focus of this study. Although the performance of the VDM

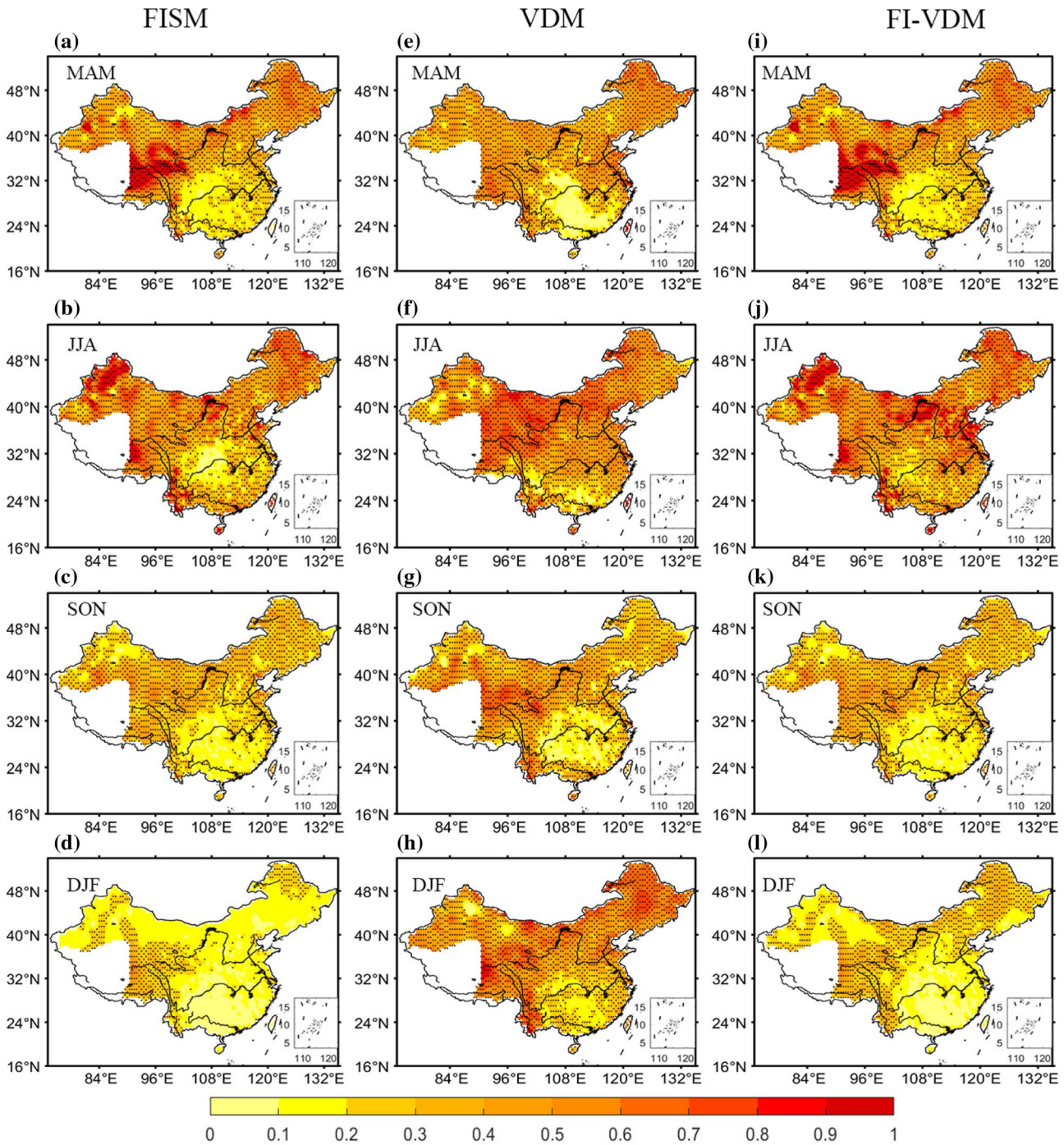

Fig. 7 Comparison of the seasonal predictability estimated by the three methods, **a**–**d** FISM, **e**–**h** VDM, and **i**–**l** FI-VDM. From the top to the bottom are the results of the four seasons: spring (March–April–May, MAM), summer (June–July–August, JJA), autumn (September–October–November, SON), and winter (December–January–February, DJF). The shading areas indicate the regions with the estimated predictability larger than 0.20

in estimating the potential predictability is comparable to that of the FI-VDM, when it comes to identifying the sources of the predictability, the shortcomings of not properly considering the climate memory effects in the VDM show up clearly. As shown in Fig. 6, the sources of predictability revealed in the leading mode of the results by the VDM alone are masked by the climate memory effects. For more meaningful patterns one needs to go further to other EOF modes (Fig. S3). In this case, however, there are still risks of misreading the results, which requires more attention.

It is worth noting that the 1729 stations are not evenly distributed. In western and northernmost China, the stations are sparser or even absent. In our analysis, interpolations are made in Figs. 4, 5, 6 and 7 according to the locations of the stations, and there is even a blank region in the southwest of China. This may induce some biases, but the stronger predictability in the vicinity of the blank area and the northernmost region is mainly related to the strong LTM over these regions (Fig. 1). Using FI-VDM, we found that the climate memory effects contribute a large portion of the seasonal predictability. This may be related to the strategy of this work, which is to extract the climate memory part first. Since the three sources of the predictability (National Research Council 2010; National Academies of Sciences, Engineering, and Medicine 2016) overlap with each other, this strategy will certainly induce a strong climate memory associated predictability. Alternative ways might exist to separate the different sources of the predictability (e.g., first estimate the climate predictability from teleconnections, then focus on the effects of the climate memory), but more detailed studies are still needed. In the end, we would like to note that the total predictability obtained from FI-VDM is an estimation of the potential predictability under the current assumption and the design of the method. The potential total predictability might be different or improved, if new assumptions are introduced, or new methodologies are applied. Therefore, to improve the seasonal predictive skills, continuous efforts on the studies of predictability are constantly required in the future.

Acknowledgements Many thanks are due to the support from the National Natural Science Foundation of China (No.41675088) and from the National Key R&D Program of China (2016YFA0600404). YQ was supported by the National Natural Science Foundation of China (No. 41675068). CF was partially supported by the Collaborative Research Centre TRR 181 "Energy Transfer in Atmosphere and Ocean", funded by the Deutsche Forschungsgemeinschaft (DFG, German Research Foundation, No.274762653). NY thanks also the support from the CAS Pioneer Hundred Talents Program.

References

Baehr J, Fröhlich K, Botzet M, Domeisen DI, Kornblueh L et al (2015) The prediction of surface temperature in the new seasonal prediction system based on the MPI-ESM coupled climate model. Clim Dyn 44:2723–2735

Brunet G, Shapiro M, Hoskins B, Moncrieff M, Dole R et al (2010) Collaboration of the weather and climate communities to advance subseasonal-to-seasonal prediction. Bull Am Meteorol Soc 91:1397–1406

Chen X, Lin GX, Fu Z (2007) Long-range correlations in daily relative humidity fluctuations: A new index to characterize the climate regions over China. Geophys Res Lett 34:L07804

Chen M, Wang W, Kumar A (2010) Prediction of monthly-mean temperature: The roles of atmospheric and land initial conditions and sea surface temperature. J Clim 23:717–725

Choi HS, Schneider UA, Rasche L, Cui J, Schmid E, Held H (2015) Potential effects of perfect seasonal climate forecasting on agricultural markets, welfare and land use: a case study of Spain. Agric Syst 133:177–189

Davies HC (2015) Weather chains during the 2013/2014 winter and their significance for seasonal prediction. Nat Geosci 8:833–837

Doi T, Behera SK, Yamagata T (2016) Improved seasonal prediction using the SINTEX-F2 coupled model. J Adv Model Earth Syst 8:1847–1867

Duan W, Song L, Li Y, Mao J (2013) Modulation of PDO on the predictability of the interannual variability of early summer rainfall over south China. J Geophys Res Atmos 118(23):13008–13021

Fraedrich K, Blender R (2003) Scaling of atmosphere and ocean temperature correlations in observations and climate models. Phys Rev Lett 90:108501

Fraedrich K, Luksch U, Blender R (2004) 1/f model for long-time memory of the ocean surface temperature. Phys Rev E 70:037301

Franzke CLE (2017) Impacts of a changing climate on economic damages and insurance. Econ Disaster Clim Change 1:95–110

Franzke CLE, Osprey SM, Davini P, Watkins NW (2015) A dynamical systems explanation of the Hurst effect and atmospheric low-frequency variability. Sci Rep 5:9068

Franzke CLE, Barbosa S, Blender R, Fredriksen H-B, Laepple T, Lambert F et al (2020) The structure of climate variability across scales. Rev Geophys 58:e2019RG000657

Frederiksen CS, Ying K, Grainger S, Zheng X (2018) Modes of interannual variability in northern hemisphere winter atmospheric circulation in CMIP5 models: evaluation, projection and role of external forcing. Clim Dyn 50:2845–2865

Fredriksen H-B, Rypdal K (2016) Spectral characteristics of instrumental and climate model surface temperatures. J Clim 29:1253–1268

Fredriksen H-B, Rypdal M (2017) Long-range persistence in global surface temperatures explained by linear multibox energy balance models. J Clim 30:7157–7168

Hasselmann K (1976) Stochastic climate models part I. Theory Tellus 28:473–485

He Z, Wu R (2014) Indo-Pacific remote forcing in summer rainfall variability over the South China Sea. Clim Dyn 42:2323–2337

He Q, Zuo Z, Zhang R, Zhang R (2018) Seasonal prediction and predictability of eurasian spring snow water equivalent in NCEP climate forecast system version 2 reforecasts. Clim Dyn 50:339–348

Jiang L, Yuan N, Fu Z, Wang D, Zhao X, Zhu X (2012) Subarea characteristics of the long-range correlations and the index χ for daily temperature records over China. Theor Appl Climatol 109:261–270

Jiang L, Li N, Zhao X (2017) Scaling behaviors of precipitation over China. Theor Appl Climatol 128:63–70

Kantelhardt JW, Koscielny-Bunde E, Rego HHA, Havlin S (2001) Detecting long-range correlations with detrended fluctuation analysis. Phys A 295:441–454

Kim H, Webster PJ, Curry JA (2012) Seasonal prediction skill of ECMWF system 4 and NCEP CFSv2 retrospective forecast for the northern hemisphere winter. Clim Dyn 39:2957–2973

Koscielny-Bunde E, Bunde A, Havlin S, Roman HE, Goldreich Y, Schellnhuber HJ (1998) Indication of a universal persistence law governing atmospheric variability. Phys Rev Lett 81:729–732

Kurnaz ML (2004) Application of detrended fluctuation analysis to monthly average of the maximum daily temperatures to resolve different climates. Fractals 12:365–373

Li Y, Li J, Feng J (2013) Boreal summer convection oscillation over the Indo-Western Pacific and its relationship with the East Asian summer monsoon. Atmos Sci Lett 14:66–71

Liu SF, Duan AM (2017) A statistical forecast model for summer precipitation in eastern China based on spring sensible heat anomaly in the Tibetan Plateau. Acta Meteorol Sin 75:903–916

Liu Y, Fan K (2012) Improve the prediction of summer precipitation in the Southeastern China by a hybrid statistical downscaling model. Meteorol Atmos Phys 117(3–4):121–134

Liu YM, Liu BQ, Ren RC, Duan AM, Mao JY (2016) Current super El Niño event and its impacts on climate in China in spring and summer. Bull Chin Acad Sci 31(2):241–250

Lovejoy S, del Rio Amador L, Hébert R (2015) The Scaling Linear macroweather model (SLIM): using scaling to forecast global scale macroweather from months to decades. Earth Syst Dyn 6:637–658

MacLeod DA, Jones A, Di Giuseppe F, Caminade C, Morse AP (2015) Demonstration of successful malaria forecasts for Botswana using an operational seasonal climate model. Environ Res Lett 10:044005

National Academies of Sciences, Engineering, and Medicine (2016) Next generation earth system prediction: strategies for subseasonal to seasonal forecasts. National Academies Press, Washington DC, p 350

National Research Council (2010) Assessment of intra-seasonal to inter-annual climate prediction and predictability. National Academies Press, Washington, DC, p 192

Peng CK, Buldyrev SV, Havlin S, Simons M, Stanley HE, Goldberger AL (1994) Mosaic organization of DNA nucleotides. Phys Rev E 49:1685–1689

Pokhrel S, Saha SK, Dhakate A, Rahman H, Chaudhari HS et al (2016) Seasonal prediction of Indian summer monsoon rainfall in NCEP CFSv2: forecast and predictability error. Clim Dyn 46:2305–2326

Qiu M, Yuan N, Yuan S (2020) Understanding long-term memory in global mean temperature: an attribution study based on model simulations. Atmos Oceanic Sci Lett (in press)

Rayner NAA, Parker DE, Horton EB, Folland CK, Alexander LV et al (2003) Global analyses of sea surface temperature, sea ice, and night marine air temperature since the late nineteenth century. J Geophys Res Atmos 108:4407

Rybski D, Bunde A, von Storch H (2008) Long-term memory in 1000-year simulated temperature records. J Geophys Res 113:D02106

Smith DM, Scaife AA, Kirtman BP (2012) What is the current state of scientific knowledge with regard to seasonal and decadal forecasting? Environ Res Lett 7:015602

Tadesse T, Haigh T, Wall N, Shiferaw A, Zaitchik B et al (2016) Linking seasonal predictions to decision-making and disaster management in the Greater Horn of Africa. Bull Am Meteorol Soc 97:ES89–ES92

Thornton H, Scaife A, Hoskins B, Brayshaw D, Smith D et al (2019) Skilful seasonal prediction of winter gas demand. Environ Res Lett 14:24009

Tommasi D, Stock CA, Pegion K, Vecchi GA, Methot RD, Alexander MA, Checkley DM (2017) Improved management of small pelagic fisheries through seasonal climate prediction. Ecol Appl 27:378–388

Vyushin DI, Kushner PJ (2009) Power-law and long-memory characteristics of the atmospheric general circulation. J Clim 22:2890–2904

Vyushin DI, Zhidkov I, Havlin S, Bunde A, Brenner S (2004) Volcanic forcing improves atmosphere-ocean coupled general circulation model scaling performance. Geophys Res Lett 31:L10206

Xie SP, Kosaka Y, Du Y, Hu K, Chowdary JS, Huang G (2016) Indo-western Pacific ocean capacitor and coherent climate anomalies in post-ENSO summer: A review. Adv Atmos Sci 33(4):411–432

Xie F, Yuan N, Qi Y, Wu W (2019) Is long-term climate memory important in temperature/precipitation predictions over China? Theor Appl Climatol 137:459–466

Ying K, Zheng X, Quan XW, Frederiksen CS (2013) Predictable signals of seasonal precipitation in the Yangtze-Huaihe River Valley. Int J Climatol 33:3002–3015

Ying K, Zhao T, Quan XW, Zheng X, Frederiksen CS (2015) Interannual variability of autumn to spring seasonal precipitation in eastern China. Clim Dyn 45:253–271

Ying K, Zhao T, Zheng X, Quan XW, Frederiksen CS, Li M (2016) Predictable signals in seasonal mean soil moisture simulated with observation-based atmospheric forcing over China. Clim Dyn 47:2373–2395

Ying K, Zheng X, Zhao T, Frederiksen CS, Quan X (2017) Identifying the predictable and unpredictable patterns of spring-to-autumn precipitation over eastern china. Clim Dyn 48:3183–3206

Yuan X, Wood EF, Luo L, Pan M (2011) A first look at climate forecast system version 2 (CFSv2) for hydrological seasonal prediction. Geophys Res Lett 38:L13402

Yuan N, Fu Z, Liu S (2013) Long-term memory in climate variability: A new look based on fractional integral techniques. J Geophys Res 118:12962–12969

Yuan N, Fu Z, Liu S (2014) Extracting climate memory using fractional integrated statisitcal model: a new perspective on climate prediction. Sci Rep 4:6577

Yuan N, Ding M, Huang Y, Fu Z, Xoplaki E, Luterbacher J (2015) On the long-term climate memory in the surface air temperature records over Antarctica: a nonnegligible factor for trend evaluation. J Clim 28:5922–5934

Yuan N, Huang Y, Duan J, Zhu C, Xoplaki E, Luterbacher J (2019) On climate prediction: how much can we expect from climate memory? Clim Dyn 52:855–864

Zheng X, Frederiksen CS (2004) Variability of seasonal-mean fields arising from intraseasonal variability: part 1, methodology. Clim Dyn 23:177–191